From Poisson's equation it follows that the Laplace transform of the electric field $E(\mathbf{q},\omega)$ is given by

$$i\mathbf{q}E(\mathbf{q},\omega)=4\pi e\sum_{\mathbf{K}'}\bar{R}_{\mathbf{K}'}(\mathbf{q},\omega), \qquad (A.10)$$

so that the electric field is given as a function of time by

$$E(\mathbf{q},t)=\frac{4\pi eq}{q^2}\int_C\left\{\sum_{\mathbf{K}'}\frac{R_{\mathbf{K}'}(\mathbf{q},0)}{\nu_{\mathbf{K}'\mathbf{q}}-\omega}\Big/H(\mathbf{q},\omega)\right\}e^{-i\omega t}\frac{d\omega}{2\pi}. \qquad (A.11)$$

It is well known from Fourier transform theory that the contour C is to be taken along a line from $-\infty$ to $+\infty$ above any singularities in the integrand.[24] For $t>0$, it is possible to close the contour by a semi-circle of infinite radius in the lower half-plane. The essential point in the derivation is the analytic continuation of the integrand into the lower half plane so that the Cauchy theorem may be used to evaluate the integral. In general, poles of the integrand in (A.11) come from both the numerator and denominator. However, the poles which are characteristic of the collective modes of the system rather than the specific form of the initial disturbance are given by the zeros of $H(\mathbf{q},\omega)$. The zeros of the analytic continuation of $H(\mathbf{q},\omega)$ into the lower half plane, give the frequency and damping rate of the damped plasma oscillations. If $H(\mathbf{q},\omega)$ has zeros in the upper half plane, the plasma oscillations undergo unstable growth. As Landau has pointed out, the analytic continuation of $H(\mathbf{q},\omega)$ may be accomplished by replacing the sum in (A.9) by an integral and suitably deforming the resulting contour. For small damping rate, this result is equivalent to the familiar prescription of replacing the resonance denominator by

$$\frac{1}{\nu_{\mathbf{K}\mathbf{q}}-\omega}=\frac{P}{\nu_{\mathbf{K}\mathbf{q}}-\omega}+i\pi\delta(\nu_{\mathbf{K}\mathbf{q}}-\omega).$$

[24] P. M. Morse and H. Feshbach, *Methods of Theoretical Physics* (McGraw-Hill Book Company, Inc., New York, 1958), p. 468.

PHYSICAL REVIEW VOLUME 125, NUMBER 3 FEBRUARY 1, 1962

Magnetoacoustic Measurements in Silver at 230 Mc/sec and 4.2°K*

VERNON J. EASTERLING AND HENRY V. BOHM
Department of Physics, Wayne State University, Detroit, Michigan
(Received September 21, 1961)

Measurements of acoustic attenuation in silver have been made with 150–233 Mc/sec longitudinal sound waves in magnetic fields up to 15 000 oersteds and at a temperature of 4.2°K. Plots of the ultrasonic pulse height as a function of the reciprocal of the magnetic field strength show from ten to fifteen maxima and minima for several orientations. Numerical data are presented and discussed in some detail. The Pippard type theoretical model of the silver Fermi surface is compared with our measurements.

INTRODUCTION

IN recent years, the oscillatory behavior of ultrasonic attenuation as a function of applied magnetic field has been reported for several metals.[1] Recent theoretical discussions[2–4] of the interaction between sound waves and electrons in very pure metals subject to a magnetic field, indicate that the observed periods of oscillation are directly related to the Fermi surface dimensions. Some preliminary magnetoacoustic data taken on silver were reported by one of us at the International Conference on the Fermi Surfaces in Metals held at Cooperstown, New York, in August, 1960.[5] Since that time, our data accuracy has been improved through development of more refined experimental techniques and the construction of higher frequency equipment. The presentation and discussion of these more recent data is the purpose of this paper.

EXPERIMENTAL TECHNIQUES

Ultrasonic pulse techniques similar to those described by Morse[6] were used. For the frequency range up to 190 Mc/sec, a commercially available[7] combination rf transmitter, receiver, and cathode-ray oscilloscope unit was used. For the frequency range from 200 to 250 Mc/sec, a new transmitter-receiver system has been constructed in our laboratory. In order to obtain more efficient transmission of power to the sample, we have found it useful to incorporate a tuned circuit into the sample mount (see Fig. 1). The sample mount, including the tuning elements, is suspended in a glass Dewar system and immersed in liquid helium. Final tuning is

* This research was supported by the U. S. Air Force through the Air Force Office of Scientific Research.

[1] Extensive discussion of recent work as well as a complete set of references may be found in *The Fermi Surface*, edited by W. A. Harrison and M. B. Webb (John Wiley & Sons, Inc., New York, 1960).

[2] A. B. Pippard, Proc. Roy. Soc. (London) **A257**, 165 (1960).

[3] M. H. Cohen, M. J. Harrison, and W. A. Harrison, Phys. Rev. **117**, 937 (1960).

[4] T. Kjeldaas and T. Holstein, Phys. Rev. Letters 2, 340 (1959).

[5] H. V. Bohm, reference 1, p. 245.

[6] R. W. Morse, *Progress in Cryogenics*, edited by K. Mendelssohn (Haywood and Company, Ltd., London, 1959), Vol. I.

[7] "Ultrasonic Attenuation Comparator" manufactured by Sperry Products, Inc., Danbury, Connecticut.

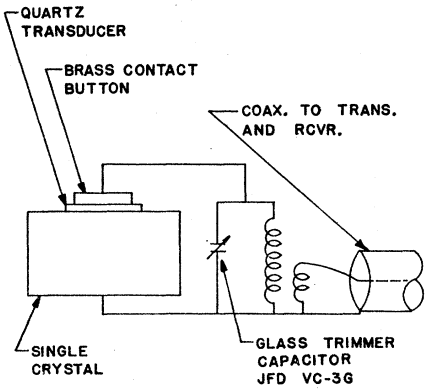

FIG. 1. Schematic of sample mounting.

then accomplished. Details of this equipment will shortly be submitted for publication elsewhere.

The magnetic field was created by a Varian model V-4012-38 rotating 12-in. magnet with 7-in. diameter pole pieces separated by a $2\frac{1}{2}$-in. gap. The maximum magnetic field obtainable was 15 000 oersteds.

The growth and preliminary preparation of the three single-crystal silver samples was done by Dr. J. F. Kirn of the Virginia Institute of Scientific Research; the raw material being 99.999% pure silver obtained from Cominco Products, Inc. Final orientation of the crystal was done by the Laue back-reflection technique; the parallel faces were aligned within one-half degree of a given major set of planes. The surfaces were polished flat and parallel to better than 0.0001 in. over the approximately three-fourths of the total sample face on which the quartz transducer was mounted.

The data were recorded by feeding a signal proportional to the monotonically varying magnetic field strength, and a signal from the receiver proportional to the ultrasonic pulse amplitude into a Honeywell-Brown "electronik duplex" two-pen recorder (linearity and accuracy of one-quarter percent of full scale).

The longitudinal sound velocities were calculated from 0°K values of elastic moduli[8] and densities. The velocities for silver as a function of orientation are: 3.515×10^5 cm/sec in the [100] direction, 3.95×10^5 cm/sec in the [110] direction, and 4.078×10^5 cm/sec in the [111] direction.

PRESENT THEORY

Cohen *et al.* have considered the attenuation of longitudinal sound waves in very pure metals in a magnetic field transverse to the direction of propagation. Using a self-consistent, semi-classical treatment of a sound wave attenuated by a free electron gas in a positive background, they predict an oscillatory dependence of the attenuation coefficient, α, as a function of $\mathbf{q}R$, where $\mathbf{q}$ is the sound wave vector $(2\pi/\lambda)$, λ is the sound wavelength, and R is the orbit radius $(\hbar kc/eH)$, $\hbar k$ being the momentum of the electron. The theoretical conditions for this oscillatory dependence are $\beta\ll1$, $ql\gg1$, in which l is the mean free path, and $\beta=\delta/\lambda$ where δ is the classical skin depth. For large qR, the oscillatory dependence of α becomes periodic and thus

$$\hbar k=\frac{\lambda e}{2c}\frac{1}{\Delta(1/H)},$$

where $\Delta(1/H)$ is the period in $1/H$, and k is an extremal distance to the Fermi surface which we shall now discuss.

The interaction of electrons with the sound wave arises largely through the induced electric field which varies sinusoidally in space with a periodicity determined by the sound wavelength. A major contribution to the electron current will arise from those portions of the electron orbits which are perpendicular to $\mathbf{q}$, and in which the electrons remain in phase with the electric field for an appreciable time. The distance along $\mathbf{q}$ between two such segments on an orbit represents a measurable dimension of the orbit. If orbits corresponding to an extremal portion of the Fermi surface have diameters of $n\lambda/2$, attenuation extrema may be expected. Recently,[9,10] there has been some discussion of the possibility that the electron moves in the crystal as though it had an effective charge e^*, different from the free electron charge e. If such is the case, then

$$\hbar k=\frac{\lambda e^*(k)}{2c}\frac{1}{\Delta(1/H)},$$

and additional information concerning e^* will be needed before a momentum calculation can be made.

FERMI-SURFACE MODEL

Experimental results reported by Shoenberg[11] (de Haas–van Alphen measurements) and Morse[12] (magnetoacoustic measurements) strongly suggest that the model proposed by Pippard[13] for copper on the basis of his anomalous skin effect study is valid for all three noble metals. The model consists essentially of a sphere pulled out in the [111] direction to make contact with the hexagonal faces of the Brillouin zone. Recently, Morse[14] has reported an indentation in the [110] direction and a bulging in the [100] direction in the Fermi surfaces of gold and copper. In the repeated zone scheme these distorted spheres join together through the "necks" along the [111] directions to form a multiple connected surface. Some of the different types of possible extremal orbits of this surface are shown in Fig. 2.

[8] J. R. Neighbours and G. A. Alers, Phys. Rev. **111**, 707 (1958).

[9] E. A. Stern, reference 1, p. 50.
[10] L. M. Falicov, reference 1, p. 58.
[11] D. Shoenberg, reference 1, p. 74.
[12] R. W. Morse, reference 1, p. 214.
[13] A. B. Pippard, Phil. Trans. Roy. Soc. London **A250**, 323 (1957).
[14] R. W. Morse, A. Myers, and C. T. Walker, J. Acoust. Soc. Am. **33**, 699 (1961).

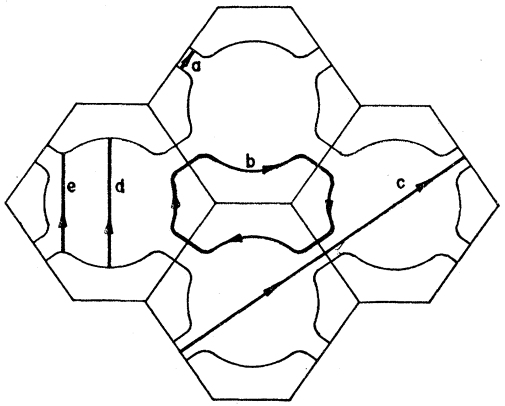

FIG. 2. Extended zone scheme showing some of the possible orbits for a Pippard-type Fermi surface; (a) neck orbit, (b) dog's bone, (c) open orbit, (d) central belly orbit, and (e) off-center belly orbit.

DATA ANALYSIS PROCEDURE

Figure 3 shows an example of the raw data on the recorder paper. The pulse height extrema (the logarithm of the pulse height is inversely proportional to the attenuation coefficient) are numbered successively and the corresponding magnetic field values are tabulated. Then a plot is made of pulse-height extremum indentification number versus the reciprocal of magnetic field strength (see Fig. 4). The slope of the straight line gives the periodicity $\Delta(1/H)$ of the oscillation. For strong clean oscillations, with ten or more extrema, the slope can be established to a fraction of one percent. Note that the points at very high and very low values of magnetic field scatter from the straight line; this behavior is predicted for the high-field points by Cohen *et al.*[3] The low-field scatter we believe to be due to experimental inaccuracies as the oscillation amplitudes become small; further, the value of $1/H$ becomes increasingly sensitive to small errors in the magnetic field reading as one goes to lower values of magnetic field.

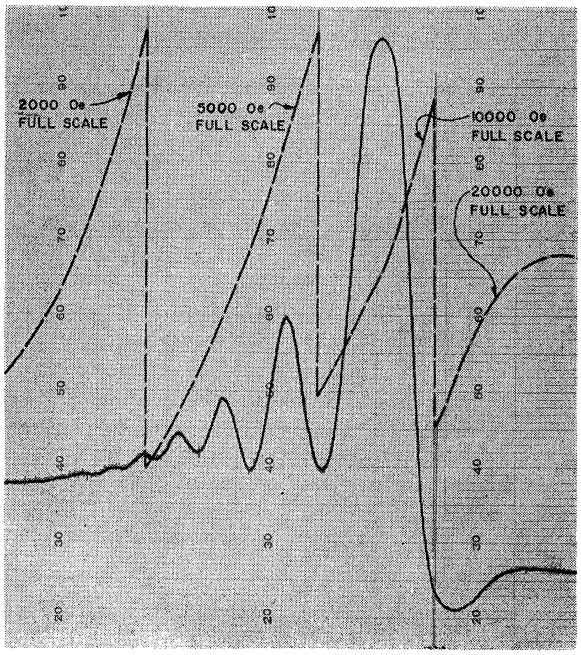

FIG. 3. Sample of data as they come from the recorder, showing the variation of the ultrasonic pulse height (solid curve) as a function of the magnetic field strength (dashed lines).

From such graphs it is possible to determine whether the observed period is for an open or closed orbit, since the conditions for maxima and minima in attenuation coefficients are exactly opposite for the two types of orbits; at infinite magnetic field, α is a maximum for closed orbits, and a minimum for open orbits. In practice, extrapolation of the line in Fig. 4 indicates that an infinite field does not correspond exactly to an extremum in α. However, in silver and copper, we have found this "phase factor" to be small enough so that there is generally little doubt as to which type of extremum should be assigned to an infinite field.

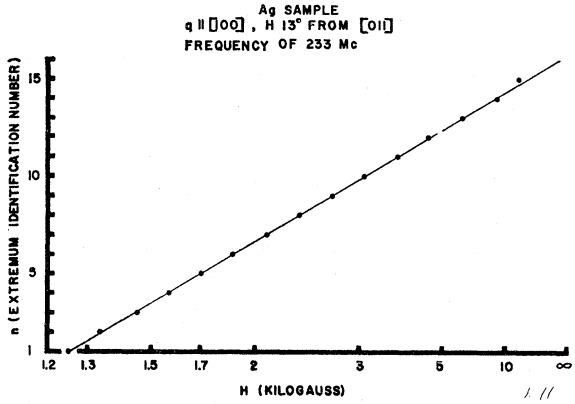

FIG. 4. Plot of extremum identification number n vs magnetic field H on a reciprocal scale. The slope of the straight line determines the period, $\Delta(1/H)$, of the magnetoacoustic oscillation.

EXPERIMENTAL RESULTS

$q \| [110]$

With $\mathbf{q} \| [110]$ and $\mathbf{H}$ rotated in a plane perpendicular to $\mathbf{q}$, the types of oscillations observed may be divided into three groups: (1) "belly" oscillations, (2) "neck" oscillations, and (3) mixed periods of oscillation. Figure 5 gives a projection of the Fermi-surface model onto a (110) plane. Here $\mathbf{q}$ is perpendicular to the figure and $\mathbf{H}$ varies in the plane of the figure. With $\mathbf{H}$ along [100] directions, strong clean oscillations are seen which give a momentum value of 1.21 (in units of 10^{-19} g cm/sec). These are interpreted as "belly"-type oscillations representing electron orbits in the region marked (d) in the figure. The angular dependence of the observed periods is shown in Table I. With $\mathbf{H}$ along a [111] direction there occurs an oscillation with a large $\Delta(1/H)$ period which gives a momentum value of approximately 0.17. This is believed to be due to "neck"

oscillations shown as region (a) in the figure. Other **H** orientations lead to mixed periods which are somewhat difficult to resolve. However, from one of the mixed periods with **H** near [110] it is possible to extract momentum values of 0.93 and 0.26 units. The 0.93 value is approximately the dimension one would expect for off-center belly orbits marked (e) in the figure. A possible interpretation of the 0.26 dimension may be that twice this value is a measure of the minimum width of the short side of the dog's bone. This interpretation implies a body radius of 1.36 units along the [100] direction. The momentum values ranging from 1.20 to 1.30 units obtained from mixed oscillations may be interpreted as due to central body orbits. Momenta in this range are found to occur where

TABLE I. Period in $\Delta(1/H)$, calculated momentum, and number of observed extrema for various magnetic field orientations for silver with 232-Mc/sec longitudinal sound wave along [110].

H orientation	Periods, $\Delta(1/H)$, in units of 10^{-4} oersted^{-1}			Momentum in units of 10^{-19} g cm/sec			Number of observed extrema
H parallel to [$\bar{1}$10]	5.04	1.53		0.27	0.89		6
H 3° from [$\bar{1}$10]	5.23	1.45		0.26	0.94		7
6°	5.04	1.31		0.27	1.04		8
9°	5.44	1.20		0.25	1.13		8
12°	5.44	1.24		0.25	1.10		10
15°	5.44	1.24		0.25	1.10		10
18°	5.44	1.13		0.25	1.21		10
21°	5.92	1.10		0.23	1.24		12
24°	8.51	1.07		0.16	1.27		11
27°	8.01	1.13		0.17	1.20		9
30°	8.01	1.06		0.17	1.29		12
33° from [$\bar{1}$10] (57° from [001])	8.01	1.62	1.03	0.17	0.84	1.32	13
54° from [001] (36° from [$\bar{1}$10])	8.01			0.17			4
51° from [001]	8.01	1.11		0.17	1.23		8
48°	8.01	1.17		0.17	1.16		8
45°	8.01	1.16		0.17	1.17		6
42°	1.22			1.12			6
39°	1.28			1.06			6
36°	1.31			1.04			6
33°	1.32			1.03			10
30°	1.35			1.01			5
27°	1.07			1.27			7
24°	1.11			1.23			7
21°	1.05			1.30			9
18°	1.06			1.29			11
15°	1.09			1.25			11
12°	1.09			1.25			11
9°	1.09			1.25			10
7°	1.12			1.22			10
5°	1.11			1.23			12
3°	1.12			1.22			13
1°	1.13			1.21			11
H parallel to [001]	1.13			1.21			13

expected, i.e., for magnetic field orientations which give central orbits that do not intersect necks. We are unable to confirm the rosette orbits which we reported previously.[5]

$q\|[100]$

The strongest oscillations are observed with $\mathbf{q}\|[100]$, and **H** varied in a (100) plane. A projection of the Fermi-surface model onto a (100) plane is shown in Fig. 6. With **H** at and near [110] directions, the electrons in the region marked (b) in the figure give rise to the dog's bone orbit which has its center of oscillation at 2.30 units from the Brillouin Zone center.[15]

[15] The lattice constant value at 4.2°K was calculated by taking the 25°C value given by C. S. Barrett, *Structure of Metals* (McGraw-Hill Book Company, Inc., New York, 1952), and correcting to 4.2°K using the thermal expansion data of F. C. Nix and D. MacNair, Phys. Rev. **61**, 74 (1942).

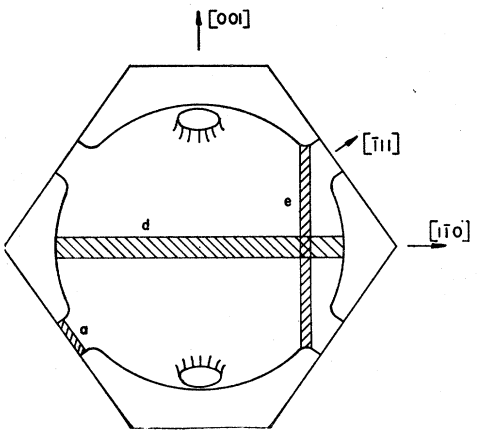

FIG. 5. Projection of Fermi-surface model onto a (110) plane. The cross-hatched regions, *a*, *d*, and *e* represent electron bands contributing to observed oscillations. The sound propagation direction is perpendicular to the plane of the figure.

Momentum values calculated from oscillations interpreted as dog's bones are measured from this point. Figure 7 shows momentum values plotted both as dog's bone interpretation and "belly" orbit interpretation. Our reason for making this type of plot is that geometrically, from the Pippard model, when **H** is moved from the [110] direction by approximately nine degrees,[16] the dog's bone orbit must disappear since an electron orbit perpendicular to **H** can no longer pass through the required four necks. Therefore, at approximately nine degrees it is necessary to begin to interpret the observed periods as coming from some other type extremal orbit. The double polar plot of Fig. 7 shows that a continuous set of experimental points is obtained

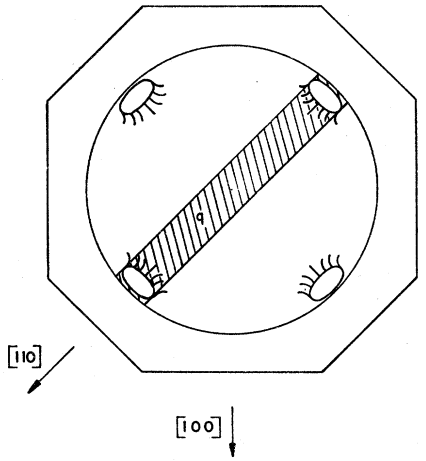

FIG. 6. Projection of Fermi-surface model onto a (100) plane. The cross-hatched region *b* represents the band of electrons contributing to the dog's bone oscillation. The sound propagation is perpendicular to the plane of the figure.

[16] Neck radii are calculated from de Haas–van Alphen data given by D. Shoenberg, Phil. Mag. **5**, 105 (1960).

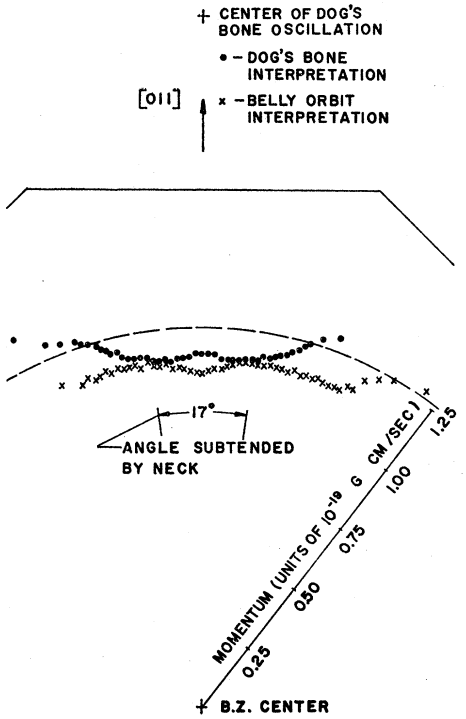

FIG. 7. Plot in (100) plane of data for silver with 233-Mc/sec longitudinal sound wave along [100] direction. The dashed line shows a free electron sphere cross section. One-half of the data plotted here is tabulated in Table II. Although symmetry exists, the other half of the experimental data was taken for checking purposes.

by changing from dog's bone to "belly" orbit interpretation near ten degrees.

In copper, plotting the data with conventional dog's bone-belly interpretation (Fig. 8) the crossover from dog's bone to belly orbit is smooth, and at the expected angle of approximately ten degrees. Also note that belly

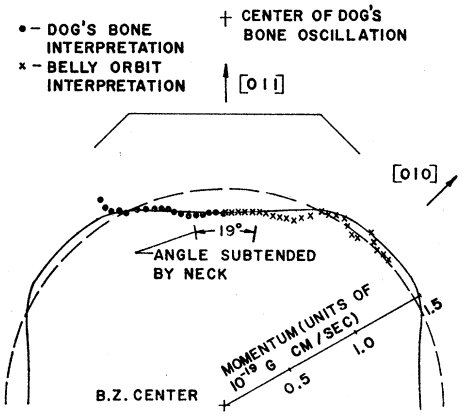

FIG. 8. Plot in (100) plane of data for copper with 233-Mc/sec longitudinal sound wave along [100] direction. The dashed line shows free electron sphere cross section and solid curve is experimental cross section reported by Morse (see reference 14). The ×'s and dots represent the same data.

orbits are observed with **H** near [100]. Table II gives the observed periods for silver and copper as a function of magnetic field orientation.[16a]

$q \| [111]$

Figure 9 shows a projection of the Fermi surface model onto a (111) plane (perpendicular to **q**). With **H** varied throughout the plane of the figure, the observed periods of oscillation change only by a few percent.

The momenta calculated from these periods as a function of angular orientation of **H** are shown in Table III. By the Pippard model, the observed periods may be interpreted as resulting from the open orbits shown in Fig. 10; then twice the calculated P value plus one-half the neck diameter should correspond to a body radius of the Fermi surface. The Fermi surface dimensions inferred from this interpretation are tabulated in Table III.

TABLE II. Data for longitudinal sound wave propagated along [100] in silver and copper at 233 Mc/sec.

	Period, $\Delta(1/H)$, in units of 10^{-4} oersted^{-1}		Momentum in units of 10^{-19} g cm/sec		Number of observed oscillations	
H orientation	Ag	Cu	Ag	Cu	Ag	Cu
H parallel to [011]	1.080	1.220	1.12	1.30	12	13
H 1° from [011]	1.080	1.230	1.12	1.29	12	13
2°	1.070	1.220	1.13	1.30	14	13
3°	1.060	1.210	1.14	1.31	12	13
4°	1.060	1.210	1.14	1.31	12	13
5°	1.070	1.210	1.13	1.31	12	13
6°	1.050	1.210	1.15	1.31	12	15
7°	1.060	1.205	1.14	1.32	12	15
8°	1.050	1.205	1.15	1.32	12	15
9°	1.035	1.195	1.17	1.33	13	15
10°	1.050	1.195	1.15	1.33	12	13
11°	1.040	1.205	1.16	1.32	12	13
12°	1.040	1.195	1.16	1.33	13	13
13°	1.040	1.175	1.16	1.35	15	13
14°	1.040	1.205	1.16	1.32	12	13
15°	1.050	1.205	1.15	1.32	13	13
16°	1.040	1.205	1.16	1.32	13	13
17°	1.050	1.205	1.15	1.32	11	13
18°	1.050	1.195	1.15	1.33	10	11
19°	1.040	1.195	1.16	1.33	10	11
20°	1.050	1.175	1.15	1.35	12	9
21°	1.050	1.175	1.15	1.35	8	9
22°	1.050	1.170	1.15	1.36	10	9
23°	1.060	1.150	1.14	1.38	7	9
24°	1.035	1.135	1.17	1.40	9	9
25°	1.035		1.17		12	
26°	0.990	1.080	1.22	1.47	13	9
28°	0.975	1.090	1.24	1.46	14	13
30°	0.960	1.065	1.26	1.49	12	13
35°	0.935	1.095	1.29	1.45	10	10
40°		1.045		1.52		7
H parallel to [010]		1.090		1.46		9

[16a] *Note added in proof.* Due to an error in the calculation of **q**, all of the experimental points for copper plotted in Fig. 8 and listed in Table II are 4% high. The corrected data shows no crossover point where a smooth transition from dog's bone to belly orbit interpretation can be made.

Using the criterion set forth under "Data Analysis Procedure," all oscillation with **q**‖[111] appear to be due to open orbits. However, a difficulty in interpretation arises when **H** is along [110], for then all central orbits must pass through four necks [see band marked (f) in Fig. 9] and the open orbit path sketched in Fig. 10 is no longer possible. One would expect that with **H** near [110] some change in the periodicity would be observed. We have taken measurements throughout this region in two-degree intervals and find no marked change in periodicity. There is another possible open orbit, for this orientation,[17] with a dimension which is determined solely by the Brillouin zone size; this orbit has a dimension value which is approximately 5% higher than that given by the data. Since relatively few extrema are observed for this orientation, this 5% difference is probably within the experimental accuracy of our silver data. However, we have also examined copper with **q**‖[111], and again find open orbits when **H** is parallel to [110] directions; further, the momentum values for this orientation (see Table III) are nearly the same as for silver, which seems to dismiss the possibility of the second type of open orbit mentioned above since the Brillouin zone for copper is greater than that for silver by 14%. In the region where orbits of the type shown in Fig. 10 are possible, the belly radii given by twice the calculated momenta plus one-half of the neck radius are in agreement with dimensions reported by Morse[12] for copper. In both silver and copper, with **H** approximately 30 degrees from [110], there is some mixing and a single peak from a second periodicity is observed; we are unable to obtain any additional information from this extra peak.

TABLE III. Data taken on silver with 233-Mc/sec longitudinal sound wave along [111] and on copper with 171-Mc/sec longitudinal sound wave along [111].

H orientation	Period, $\Delta(1/H)$, in units of 10^{-4} oersted^{-1}		$P_\perp$, calculated momenta (units of 10^{-19} g cm/sec)		$2P_\perp$ + neck radius (neck radii taken to be 0.18 for Ag and 0.29 for Cu)[a]		Number of observed extrema	
	Ag	Cu	Ag	Cu	Ag	Cu	Ag	Cu
Parallel to [1$\bar{1}$0]	2.34	4.050	0.60	0.61			4	5
2° from [1$\bar{1}$0]	2.34	4.050	0.60	0.61			5	5
4° from [1$\bar{1}$0]	2.34		0.60				4	
6°	2.34	4.050	0.60	0.61			7	5
8°	2.50		0.56				7	
10°	2.55	4.495	0.55	0.55	1.28	1.39	7	5
12°	2.70		0.52		1.22		6	
14°	2.60		0.54		1.26		6	
16°	2.75	4.495	0.51	0.55	1.20	1.39	4	5
18°	2.60		0.54		1.26		7	
20°	2.42		0.58		1.34		6	
22°	2.42	4.415	0.58	0.56	1.34	1.41	6	5
24°	2.38		0.59		1.36		5	
26°	2.50		0.56		1.30		5	
28°	2.34		0.60		1.38		5	
30° from [1$\bar{1}$0]	2.42	4.660	0.58	0.53	1.34	1.35	5	5

[a] Neck radii calculated using de Haas–van Alphen measurements given in reference 16.

[17] We wish to thank Dr. W. A. Harrison of the General Electric Research Laboratories for bringing this possible orbit to our attention.

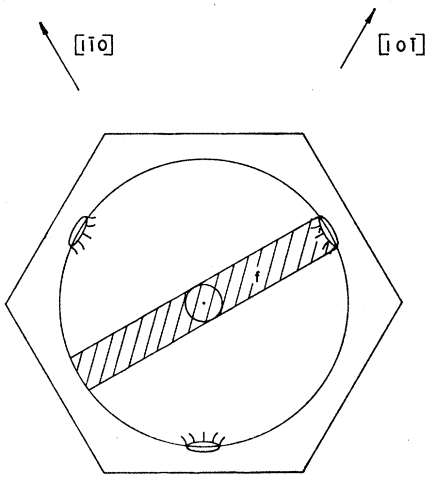

FIG. 9. Projection of Fermi surface model onto (111) plane. The sound propagation direction is perpendicular to the plane of the figure.

DISCUSSION

It is to be noted that the accuracy of the data varies a great deal depending on sound propagation direction and magnetic field orientations. Very accurate periods can be obtained for the dog's bone and belly oscillations obtained with **q**‖[100] and **H** within 20 degrees of [110], and also for the belly oscillations with **q**‖[110] and **H** within 20 degrees of [100]. For these orientations there are ten or more extrema and almost all of the points fall on the straight line on an n vs $1/H$ plot similar to that shown in Fig. 4. Data from all other orientations exhibit either a small number of oscillations or mixed periods, and are estimated to be good within 5%.

Our data are in agreement with the Pippard model with respect to the existence of the dog's bone oscillation with **q**‖[100], the neck oscillation with **q**‖[110], and open orbits with **q**‖[111]. However, there still appears to be a possible discrepancy in the existence of open orbits with **q**‖[111] and **H**‖[110]. Presently, we observe very few oscillations in this region; future experiments at higher frequencies may clarify the situation.

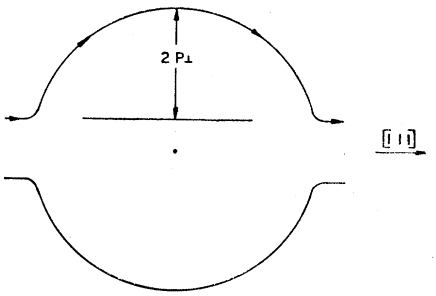

FIG. 10. Open orbit with **q**‖[111]. $2P_\perp$ plus one-half of the neck diameter gives a main body radius.

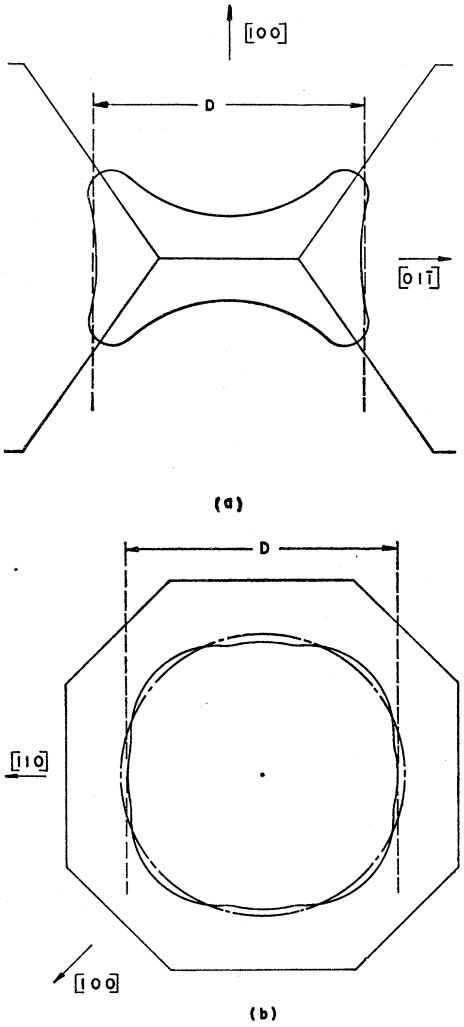

FIG. 11. Orbit shapes for (a) dog's bone with $\mathbf{q}\|[100]$ and $\mathbf{H}\|[011]$ and (b) belly oscillation with $\mathbf{q}\|[110]$ and $\mathbf{H}\|[001]$. The broken line in figure (b) represents a free-electron sphere. The dimension D is that measured by the magnetoacoustic effect.

It is of interest to discuss the data from the two regions giving strong oscillations, both of which give the Fermi-surface dimension along [110] directions. The fact that the belly oscillation with $\mathbf{q}\|[110]$ gives a dimension which is $2\frac{1}{2}\%$ higher than that inferred from the dog's bone oscillation may be explained by examining the orbit shapes as shown in Fig. 11. The shape of the end of the dog's bone orbit [Fig. 11(a)] is experimentally determined by the magnetic field orientation dependence of the belly orbit dimension (with $\mathbf{q}\|[110]$), and similarly the shape of the belly orbit [Fig. 11(b)] is found by examining the magnetic field orientation dependence of the dog's bone and belly orbit dimensions occurring with $\mathbf{q}\|[100]$. It is reasonable to take the measured periods of oscillation to represent the dimensions marked D in the figure; thus, the period given by the orbit in Fig. 11(a) implies a [110] radius which is slightly small, whereas the belly period from the orbit shown in Fig. 11(b) should give a more accurate measurement. Further theoretical clarification of precisely which "electron strips" are important to the magnetoacoustic effect would be helpful.

TABLE IV. Comparisons of experimentally determined values of qR at extrema in α, with values predicted by theory of Cohen, Harrison, and Harrison (CHH). Experimental points are for $\mathbf{q}\|[100]$, $\mathbf{H}$ 13° from [011], and a frequency of 233 Mc/sec.

qR at maxima			qR at minima		
CHH	exp.	Δ=CHH−exp.	CHH	exp.	Δ=CHH−exp.
0.00	···	···	2.94	2.35	0.59
4.04	3.40	0.64	6.04	5.08	0.96
7.27	6.72	0.55	9.16	8.21	0.95
10.45	9.79	0.66	12.28	11.37	0.91
13.61	12.96	0.65	15.41	14.52	0.89
16.77	16.19	0.58	18.55	17.71	0.84
19.92	19.29	0.63	21.68	20.78	0.90
23.07	22.62	0.45	24.82	24.16	0.66

Cohen *et al.*[3] have calculated the theoretical qR positions of maxima and minima in the ultrasonic attenuation coefficient (Table IV), for the case of $ql \gg 1$. Kjeldaas and Holstein[4] have considered the intermediate case for ql on the order of 3 to 15 and find no appreciable shift in the positions of the maxima and minima but do predict a damping out of the oscillations and a reduction in the saturation attenuation at high fields as ql is reduced. If we take the mean free path l to be approximately equal to one-half of the circumference of the orbit giving rise to resonance at the lowest magnetic field (i.e., $l \simeq n\pi\lambda/2$, where n is the number of observed maxima in α), then we obtain a ql of about 50. On the other hand, the relative values of α at high and zero magnetic fields[3,4] indicate that our sample has a ql value just above $5\pi/2$. The reason for this difference is not clear. The theoretical values of qR at extrema in α have been compared with those determined experimentally for several orientations and a typical set of values is shown in Table IV. The shift (Δ in the Table) of the experimental values from those predicted by theory is different for maxima and minima. Thus, it appears that the experimental data gives an α vs qR curve with successive extrema which are evenly spaced, whereas the theoretical curve has the minima shifted towards high qR.

ACKNOWLEDGMENTS

The authors gratefully acknowledge several interesting discussions with Dr. W. A. Harrison of the General Electric Research Laboratory and Dr. W. A. Overhauser of the Ford Motor Company Scientific Laboratory. We wish to thank N. H. Horwitz of the Wayne State University Physics Research Laboratory for his assistance in the construction of the equipment.

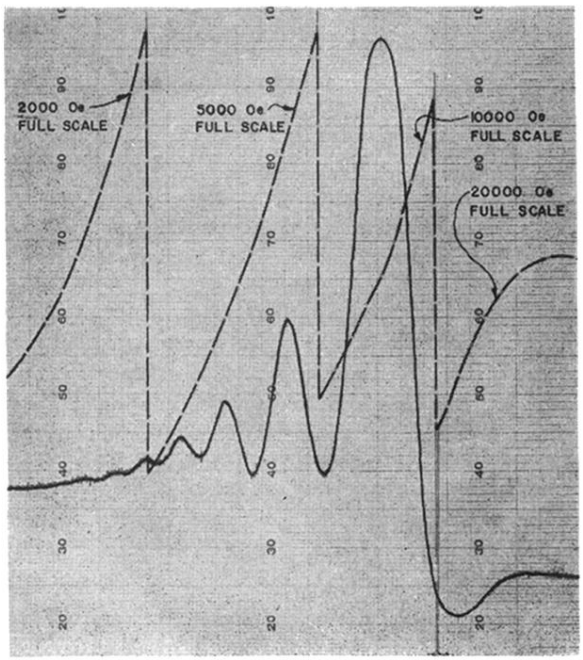

FIG. 3. Sample of data as they come from the recorder, showing the variation of the ultrasonic pulse height (solid curve) as a function of the magnetic field strength (dashed lines).